Synthesis, characterization, crystal structure and HSA binding of two new N,O,O-donor Schiff-base ligands derived from dihydroxybenzaldehyde and tert-butylamine

Iman Khosravi, Farnaz Hosseini, Mahsa Khorshidifard, Mehdi Sahihi, Hadi Amiri Rudbari

Synthesis, characterization, crystal structure and HSA binding of two new N,O,O-donor Schiff-base ligands derived from dihydroxybenzaldehyde and *tert*-butylamine

Iman Khosravi [a], Farnaz Hosseini [b], Mahsa Khorshidifard [b], Mehdi Sahihi [b], Hadi Amiri Rudbari [b]

[a] Department of Chemistry, Qeshm Branch, Islamic Azad University, Qeshm, Iran

[b] Department of Chemistry, University of Isfahan, Isfahan 81746-73441, Iran

Abstract

Two new *o*-hydroxy Schiff-bases compounds, **L^1** and **L^2**, were derived from the 1:1 M condensation of 2,3-dihydroxybenzaldehyde and 2,4-dihydroxybenzaldehyde with *tert*-butylamine and were characterized by elemental analysis, FT-IR, ^{1}H and ^{13}C NMR spectroscopies. The crystal structure of **L^2** was also determined by single crystal X-ray analysis. The crystal structure of **L^2** showed that the compound exists as a zwitterionic form in the solid state, with the H atom of the phenol group being transferred to the imine N atom. It adopts an *E* configuration about the central C N double bond. Furthermore, binding of these Schiff base ligands to Human Serum Albumin (HSA) was investigated by fluorescence quenching, absorption spectroscopy, molecular docking and molecular dynamics (MD) simulation methods. The fluorescence emission of HSA was quenched by ligands. Also, suitable models were used to analyze the UV–vis absorption spectroscopy data for titration of HSA solution by various amounts of Schiff bases. The spectroscopic studies revealed that these Schiff bases formed 1:1 complex with HSA. Energy transfer mechanism of quenching was discussed and the values of 3.35 and 1.57 nm as the mean distances between the bound ligands and the HSA were calculated for **L^1** and **L^2**, respectively. Molecular docking results indicated that the main active binding site for these Schiff bases ligands is in subdomain IB. Moreover, MD simulation results suggested that this Schiff base complex can interact with HSA, with a slight modification of its tertiary structure.

Keywords

Schiff base ligands

Crystal structure

HSA binding

Molecular docking

Molecular dynamics simulation

1. Introduction

o-Hydroxy Schiff-bases compounds are important class of compounds from crystallography and biological activity points of view. From the crystallography point of view, o-hydroxy Schiff bases represent an important class of compounds that are of great interest to the investigators

mostly because of the intramolecular H-bond. *o*-Hydroxy Schiff-bases compounds display two possible tautomeric forms, the phenol-imine (OH) and the keto-amine (NH) forms. Depending on the tautomers, two types of intramolecular hydrogen bonds are observed in Schiff bases: O H···N in phenol-imine and N H···O in keto–amine tautomers [1], [2], [3].
In the latter case, a proton transfer may cause a change in the electron structure: the electronic and protonic states are clearly coupled, and an intramolecular charge transfer may occur. Hence, a zwitterionic structure may appear, which is rarely seen for hydroxy derivatives. The characteristic property of this form is the presence of ionic N^{+}–H···O^{-} hydrogen bond [4], [5].

The previous research showed that the position of the proton in the OH···N– region dramatically affects the interactions and plays a very important role in determining the physical, chemical properties of o-hydroxy Schiff bases. In this regard, we can mention to photo-, thermo-, and solvatochromic properties [6] and a variety of their applications were revealed in both theoretical and experimental investigations [7], [8], [9], [10], [11], [12].
From the biological activity perspective, the origin of biological activity, especially anticancer activity of Schiff bases has been attributed to their ability to cleave DNA. It has been proved that in Schiff bases compounds the HC N linkage is an essential structural requirement for biological activity. Since Schiff bases are potential anticancer drugs, it was of interest to obtain insight in to their modes of binding with the most abundant plasma carrier protein, Human Serum Albumin (HSA), using spectroscopic techniques and molecular modeling [13], [14], [15], [16], [17], [18].
Fluorescence and UV–vis absorption spectroscopy are effective techniques to study the drug–protein interactions, because of their sensitivity, reproducibility and convenience. These approaches can reveal the binding affinity of small molecules with proteins and help to understand their binding mechanisms [13], [14], [15], [16], [17], [18]. Furthermore, it was of interest to locate binding sites of drugs on HSA. It requires docking tools that are able to identify the pose of the molecule in the binding site and the binding affinity or a score representing the strength of binding [13], [14], [15], [16], [17], [18].
As part of our ongoing investigation into designing new Schiff base ligands and complexes [13], [19], [20], [21], [22], [23], [24], [25], [26], [27], [28], [29], [30], [31], [32], [33], herein we present results of a detailed investigation on the synthesis and structural characterization of two new o-hydroxy Schiff bases ligands derived from the condensation of *tert*-butylamine with 2,3-dihydroxybenzaldehyde (**L^1**) and 2,4-dihydroxybenzaldehyde (**L^2**) using IR, NMR, elemental analysis and single-crystal X-ray diffraction. In addition, the interaction between Schiff base ligands and HSA has been investigated using spectroscopic methods-fluorescence, UV absorption-along with the protein–ligand docking and molecular dynamics simulation techniques.

2. Experimental section

2.1. Chemicals and instrumentation

Human serum albumin (HSA) was purchased from Sigma–Aldrich. 2,3-dihydroxybenzaldehyde, 2,4-dihydroxybenzaldehyde and *tert*-butylamine were obtained from Merck Co. and used without

further purification. All of the solutions were used freshly after preparation. The FT-IR spectra were recorded on a JASCO, FT/IR-6300 spectrometer (4000–400 cm^{-1}) in KBr pellets.
^{1}H and ^{13}C NMR spectra for **L^1** and **L^2** were recorded on a Bruker Avance 400 spectrometer using $CDCl_3$ and DMSO-d_6 as solvent, respectively. The elemental analysis was performed on Leco, CHNS-932 and Perkin–Elmer 7300 DV elemental analyzers. The UV–vis spectra were recorded on a JASCO V-670 spectrophotometer. Fluorescence measurements were carried out on Shimadzu RF-5000 spectrofluorometer at room temperature.

2.2. Single crystal diffraction studies

The crystallographic data for Schiff base ligand, **L^2**, was collected at room temperature with a Bruker APEX II CCD area detector diffractometer using Mo-Kα radiation (0.71073 Å). Data collections, cell refinements, data reductions and absorption corrections were performed using multiscan methods with Bruker software [34]. The structures were solved by direct methods using SIR2004 [35]. The non-hydrogen atoms were refined anisotropically by the full matrix least squares method on F^2 using SHELXL [36].

Hydrogen atoms for CH and CH_3 groups were positioned geometrically (C H = 0.93 Å for

CH, C H = 0.96 Å for CH_3) and refined using a riding model. H atoms of NH group was found in difference Fourier map and refined isotropically. Molecular graphics were prepared with the Olex2 program [37]. Crystallographic data for **L^2** are listed in Table 1. Selected bond distances and angles are summarized in Table 2.
Table 1. Crystal data and structure refinement for **L^2**.

Empirical formula	$C_{11}H_{15}NO_2$
Formula weight	193.24
Temperature (K)	298(2)
Wavelength (Å)	0.71073
Crystal system	Orthorhombic
Space group	$P2_12_12_1$
Unit cell dimensions	a = 7.6122(15)
	b = 11.962(2)
	c = 12.631(3)
Volume ($Å^3$)	1150.1(4)

Z	4
Calculated density (Mg/m^3)	1.116
Absorption coefficient (mm^{-1})	0.077
F(000)	416
Theta range for data collection (°)	3.12 to 24.99
Index ranges	$-9 \leq h \leq 9$
	$-14 \leq k \leq 14$
	$0 \leq l \leq 15$
Reflections collected	3770
Independent reflections	2023 [$R_{(int)} = 0.0200$]
Data Completeness (%)	99.9
Refinement method	Full-matrix least-squares on F^2
Data/restraints/parameters	2023/0/138
Goodness-of-fit on F^2	0.896
Final R indices [$I > 2\sigma(I)$]	$R_1 = 0.0286$
	$wR_2 = 0.0642$
R indices (all data)	$R_1 = 0.0367$
	$wR_2 = 0.0657$
Largest diff. peak and hole ($e.Å^{-3}$)	0.064 and −0.142

Table 2. Selected bond lengths (Å) and angles (°) for **L²**.

O(1)	C(2)	1.299(2)

O(2)	C(4)		1.342(2)
N(1)	C(7)		1.298(2)
N(1)	C(8)		1.482(2)
C(1)	C(7)		1.403(2)
C(7)	N(1)	C(8)	128.0(1)
O(2)	C(4)	C(3)	123.4(1)
O(2)	C(4)	C(5)	116.1(1)
O(1)	C(2)	C(3)	122.7(1)
O(1)	C(2)	C(1)	120.1(1)
N(1)	C(7)	C(1)	124.7(1)
C(7)	C(1)	C(6)	119.5(1)
C(4)	O(2)	H(2)	109 (1)
C(8)	N(1)	H(1)	119(1)
C(7)	N(1)	H(1)	113(1)

2.3. Synthesis of Schiff-base ligands

Tert-butylamine (10 mmol) was dissolved in 30 mL of absolute methanol and added slowly to a stirred solution 2,3-dihydroxybenzaldehyde or 2,4-dihydroxybenzaldehyde (10 mmol) in 30 mL of absolute methanol in ambient temperature. The color immediately changed to yellow for **L[1]** and orange for **L[2]**. The mixture was then stirred for 2 h in ambient temperature. The reaction mixture was allowed to stand for slow evaporation of the solvent until the formation of precipitate. The precipitate was filtered off and purified by washing with 10 mL of cold methanol. For compound **L[2]**, the filtrate was allowed to stand at room temperature and orange crystals suitable for single crystal X-ray diffraction analysis were obtained after 1–2 days.
L[1]: Yield: 91%. Anal. calc. for $C_{11}H_{15}NO_2$: C: 68.37, H: 7.82, N: 7.25. Found: C: 68.32, H: 7.80, N: 7.29. ^{1}HNMR ($CDCl_3$, 400 MHz, 298 K) δ/ppm: 14.73 (1H, br, O*H*); 8.10 (s, 1H, N C*H*); 6.91 (d of d), 6.70 (d of d), 6.48 (t) (3H, H_{ar}); 1.47 (s, 9H, CH_3). ^{13}CNMR ($CDCl_3$, 400 MHz, 298 K) δ/ppm: 159.89 (*C*H N), 148.18, 122.15, 115.00, 114.56, 113.54 (Ar carbons), 55.73 (*C*H$(CH_3)_2$), 29.54 (CH(*C*$H_3)_2$. FT-IR: Selected IR data (KBr, cm^{-1}): 1636(νC = N), 1185(νC–O).
L[2]: Yield: 93%. Anal. calc. for $C_{11}H_{15}NO_2$: C: 68.37, H: 7.82, N: 7.25. Found: C: 68.35, H: 7.85, N: 7.30. ^{1}HNMR (DMSO-d_6, 400 MHz, 298 K) δ/ppm: 14.70 (1H, br, O*H*); 8.39 (s, 1H, N C*H*); 7.23(d), 6.23 (d), 6.11 (d) (3H, H_{ar}); 3.46 (1H, br, N*H*); 1.34 (s, 9H, CH_3).^{13}CNMR (DMSO-d_6, 400 MHz, 298 K) δ/ppm: 162.06 (*C*H N), 159.63, 133.85, 110.90, 106.22, 102.94 (Ar carbons), 55.29 (*C*H$(CH_3)_2$), 29.35 (CH(*C*$H_3)_2$. FT-IR: Selected IR data (KBr, cm^{-1}): 1636(νC N), 1204(νC–O).

2.4. HSA binding experiments

A stock solution of HSA was prepared by dissolving the desired amount of HSA in 50 mM phosphate buffer (pH = 7). The HSA stock solution was stored at 4 °C in the dark and used within 2 h. HSA concentration was determined by UV–vis spectroscopy using the molar absorption coefficient 35,700 M^{-1} cm^{-1} at 278 nm [38]. The solution of the compounds was first prepared in DMSO as co-solvent, and then diluted with phosphate buffer. The final DMSO concentration never exceeded 0.5% v/v. All the solutions were used freshly after preparation. The interaction of HSA with the synthesized Schiff base ligands was investigated using absorption titration experiment at room temperature. The UV–vis absorption spectra of the solution of HSA (10 μM) in the absence and presence of various amounts of the ligands (100 μM) were recorded at room temperature and the changes in the HSA absorption were recorded after each addition. Moreover, fluorescence quenching experiment was also done to more investigation of the interaction between HSA and the Schiff base ligands. In this experiment 2 mL of HSA solution (5 μM) was placed into the cell and various amounts of the Schiff base ligands (50 μM) were added to the cell. The absorbance at excitation wavelengths was always less than 0.1, in order to avoid inner filter effects. The fluorescence intensity was measured with excitation wavelength at 295 nm and emission wavelength rang of 300–450 nm and the excitation and emission slits set at 5 and 10 nm, respectively. In each measurement the mixture was allowed to incubate for 2 min after addition of the ligand.

2.5. Molecular docking procedure

In this work, docking study was carried out to indicate the binding site for the synthesized ligands. The 3D structures of the **L²** ligand was generated using the CIF file of its X-ray crystal structure. The CIF file was converted to the PDB format by using the Mercury software (http://www.ccdc.cam.ac.uk/). The geometry of the **L¹** ligand was optimized using Gaussian 03 [39] at the level of B3LYP/6-31G** [40], [41]. The crystal structure of HSA (PDB ID: 1AO6) was taken from the Brookhaven Protein Data Bank (http://www.rcsb.org/pdb). The R-value and resolution of this file were 0.218 and 0.25 Å, respectively. Water molecules of the protein. pdb file were removed, polar hydrogen atoms and Gasteiger charges were added. Flexible-ligand docking was performed by AutoDock 4.2 molecular-docking program using the implemented empirical free energy function and the Lamarckian Genetic Algorithm [42]. The Autogrid was used to calculate Grids. A blind docking with 126 lattice points along X, Y, and Z axes was performed to find the active site of ligands on HSA. After determination of the active site, the dimensions of the grid map were selected 60 points with a grid point spacing of 0.375 Å, to allow the ligand to rotate freely. 200 docking runs with 25,000,000 energy evaluations for each run were performed.

2.6. Molecular dynamics simulation

The lowest binding free energy conformation of each complex was considered as the initial conformation for the MD studies. All MD studies were carried out using the GROMACS 4.5.6 (University of Groningen, Netherlands) package [43], [44] and the GROMOS96 43a1 force field [45], [46]. The Dundee PRODRG2.5 server was used to generate the topology parameters of the ligands [47]. The partial atomic charges of ligands were calculated using Gaussian 03 [39] at the level of B3LYP/6-31G** [40], [41]. The complex was located in the cubic box with the periodic boundary conditions. The box volume was 11.36381 × 11.36381 × 11.36381 nm^3 and the minimum distance between the protein surface and the box was 1.0 nm. The box, filled with extended simple point charges (SPC), water molecules [48], and the solvated systems, were neutralized by adding 15 sodium ions (Na^+). Energy minimization was done through using the steepest descent method. Then, the system was equilibrated for 100 ps at the temperature of 300 K. Finally, a 20 ns MD simulation was carried out at 1 bar and 300 K. A Berendsen thermostat [49] at 300 K, the particle mesh Ewald (PME) method [50], [51] for long range electrostatics, and a 9 Å cut off for van der Walls interactions and Coulomb interactions were used. The equation of motions was integrated by the leap-frog algorithm with the 2 fs time steps. The atomic coordinates were recorded to the trajectory file every 0.5 ps for later analysis. Finally, an all-bond constraint was used to keep the ligand from drifting in the MD.

3. Results and discussion

The procedure synthesis of the Schiff base ligands, **L¹** and **L²**, reported in Scheme 1. The **L¹** and **L²** Schiff base ligands obtained by the self-condensation reaction between *tert*-butylamine with 2,3-dihydroxybenzaldehyde (**L¹**) and 2,4-dihydroxybenzaldehyde (**L²**), respectively, in methanol at the ambient temperature. The Schiff base ligands are yellow (**L¹**) and orange (**L²**) powder, stable in air and soluble in the most common organic solvents such as MeOH, EtOH, $CHCl_3$, DMSO, DMF.

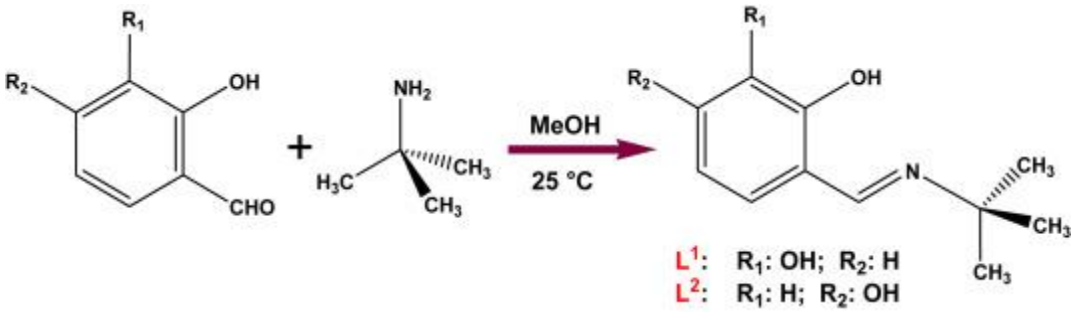

Scheme 1. Synthesis of Schiff base ligands.

The most characteristic feature in the IR spectra of the Schiff base ligands comes from the C N stretching vibrations. In IR spectra, these stretching vibrations are at 1636 cm^{-1} for **L¹** and **L²** confirming the presence of the imine groups. The presence of several medium intensity bands in the range 3060–2740 cm^{-1} suggests the existence of C H stretching vibrations of aliphatic and aromatic protons. Another characteristic region of the Schiff bases derivate spectrum is 1100–1400 cm^{-1}, which is attributed to C O stretching vibrations. The C O stretching vibration was observed at 1185 $cm^{-1}$and 1204 cm^{-1} for **L¹** and **L²** respectively, which confirms the presence of phenolate group in the compound. Also, The Schiff base ligands exhibit two broad IR-bands of medium intensity in the 3400–3200 cm^{-1} region, the higher frequency peak is due to the ν(OH) mode while the lower one can be assigned to the ν(N H) vibration [21]. The presence of the OH and NH hydrogens are also revealed in the X-ray crystal structure of the **L²** ligand.

The ^{1}H NMR and ^{13}C NMR spectra of **L¹** and **L²** were recorded using $CDCl_3$ (**L¹**) and DMSO-d_6 (for **L²**) as the solvent and data are summarized in the experimental section and shown in Fig. 1, Fig. S1 and Fig. S2. The ^{1}H and ^{13}C NMR spectra were run immediately after solution in $CDCl_3$ (**L¹**) and DMSO-d6 (for **L²**) with TMS as internal standard and gave the expected simple spectra, indicating the integrity of the Schiff base ligands. The spectra obtained after 12, 24 and 120 h were similar to the initial spectra indicating that the Schiff base ligands are stable in solution.

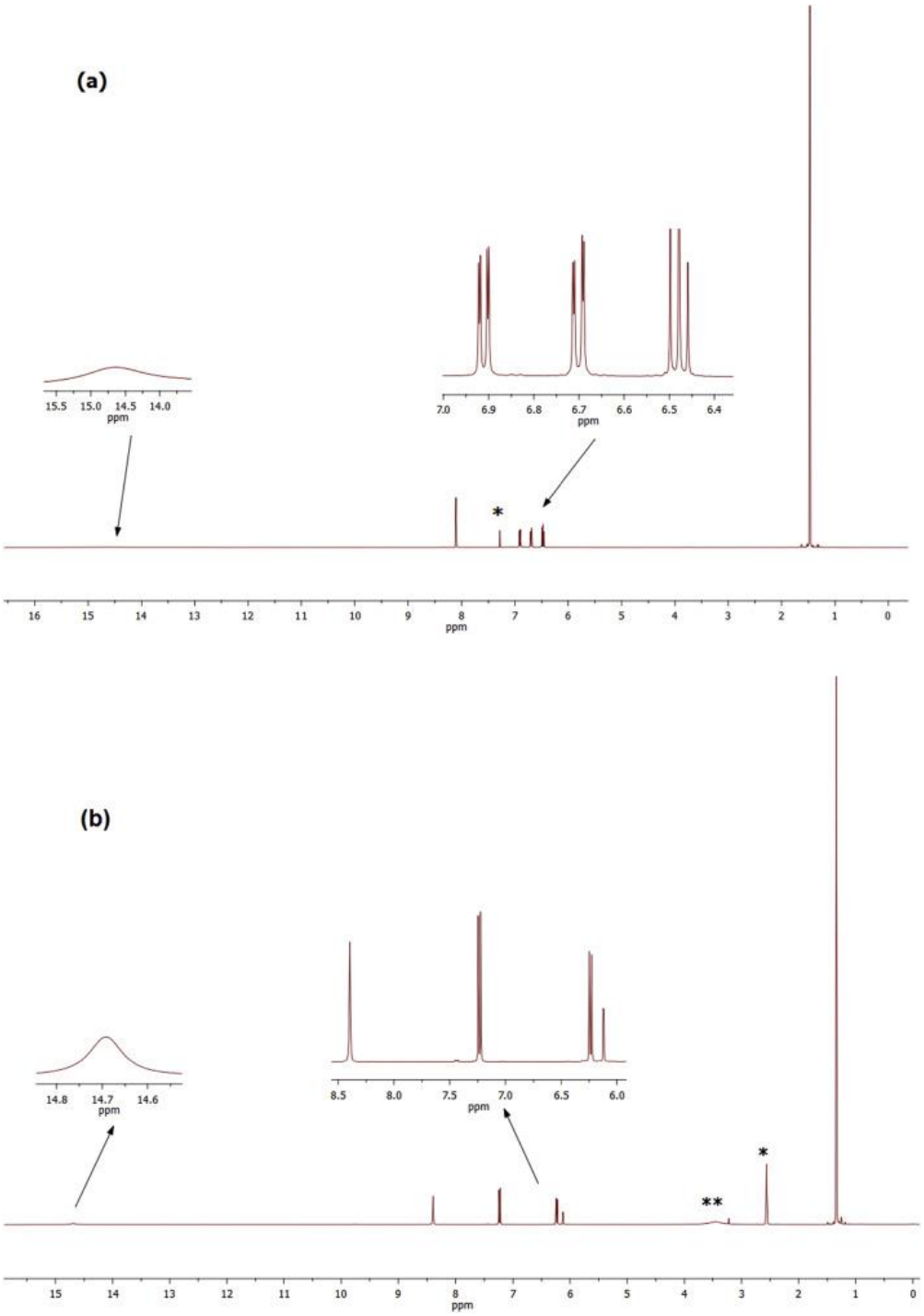

Fig. 1. ^{1}HNMR of (a) **L^{1}** and (b) **L^{2}**. A star marks in black color represents peak for $CDCl_3$ (**L^{1}**) and DMSO-d_6 (**L^{2}**).

The ^{1}H NMR spectra of **L^{1}** and **L^{2}** Schiff base ligands exhibit $–OH_{phenolic}$ proton resonances at ~14.70 ppm for two $–OH_{phenolic}$ protons as broad singlet peak (Fig. 1). The signal for the imine proton in the **L^{1}** and **L^{2}** Schiff base ligands appears at 8.10 and 8.39 ppm, respectively, as a singlet

peak. Also, methyl protons appear as singlet at 1.47 and 1.34 ppm for **L¹** and **L²**, respectively. ^{13}C NMR spectra of Schiff base ligands, **L¹** and **L²**, show in the region corresponding to signals of aromatic rings (148.18–113.54 ppm for **L¹** and 159.63–102.94 ppm for **L²**) 5 peaks instead of 6 expected peaks are observed. It seems that one carbon in this region are overlapping to other carbons due to high similarity of carbons (See Figs. S1 and S2). Also, ^{13}C NMR spectra show the azomethine carbon peaks at 159.89 and 162.06 ppm, for **L¹** and **L²**, respectively.

The UV–vis electronic absorption spectra of the title compounds were recorded in MeOH solvent. The experimental diagrams of absorption spectra for two Schiff base compounds are shown in Fig. 2. The observed spectra showed four bands at 210, 231, 288 and 381 nm for **L¹** and three bands at 221, 299 and 371 nm for **L²**. It should be noted that the electronic absorption spectra of 2-hydroxy Schiff bases which exist mainly as phenol–imine structure indicate the presence of a band at <400 nm, whereas compounds that existing in the keto–amine form show a new band, especially in polar and nonpolar solvents at >400 nm [52], [53], [54]. According to absence of bonds at >400 nm in UV–vis spectra of two compounds, we can say that the compounds exist in solution as phenol–imine form. This result also can be confirmed by ^{1}HNMR spectra (Fig 1). As a result, the observed bands at 210, 231, 288 and 381 nm for **L¹** and three bands at 221, 299 and 371 nm for **L²** can be due to benzene $\pi \rightarrow \pi^*$ and azomethine $\pi \rightarrow \pi^*$ and $n \rightarrow \pi^*$ transitions. These values are similar to those found in related compound [55], [56].

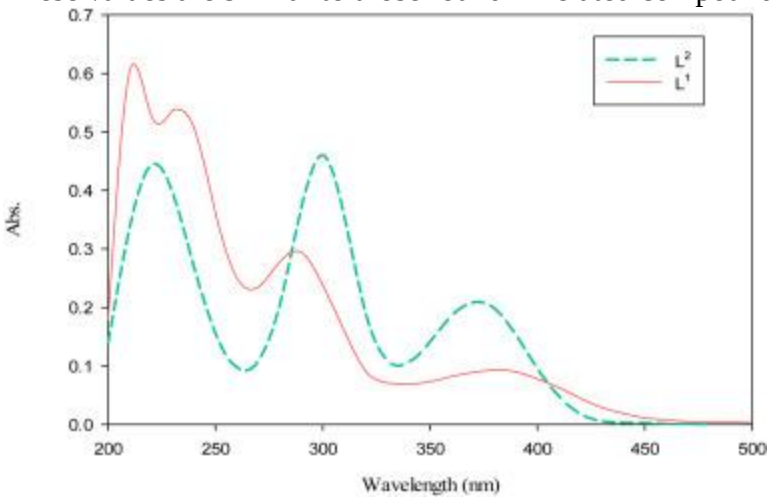

Fig. 2. UV–Vis spectra of **L¹** (a) and **L²** (b) in MeOH solution at 25 °C.

3.1. Crystal structure of L^2

The molecular structure of **L²** is shown in Fig. 3. Selected bond distances and bond angles are listed in Table 2. The molecule has adopted E-configuration about the C7 N1 double bond (1.2981(18) Å) with a C8 N1 C7 C1 torsion angle of 178.139°. The C11 N1 [1.300(4) A] and C2 O1 [1.304(4) A] bonds of the title compound are the most important indicators of the tautomeric type (Scheme 2). While the C2 O1 bond is of a double bond for the keto–amine tautomer, this bond displays single bond character in phenol–imine tautomer. In addition, the C11 N1 bond is also a double bond in phenol–imine tautomer and of single bond

length in keto–amine tautomer [53], [57]. However, these bond distances have intermediate values between single and double C O (1.362 and 1.222 A, respectively) and C N (1.339 and 1.279 A, respectively) bond distance. The shortened C2 O1 bond and the slightly longer C11 N1 bond provide structural evidence for the zwitterionic form of the title compound.

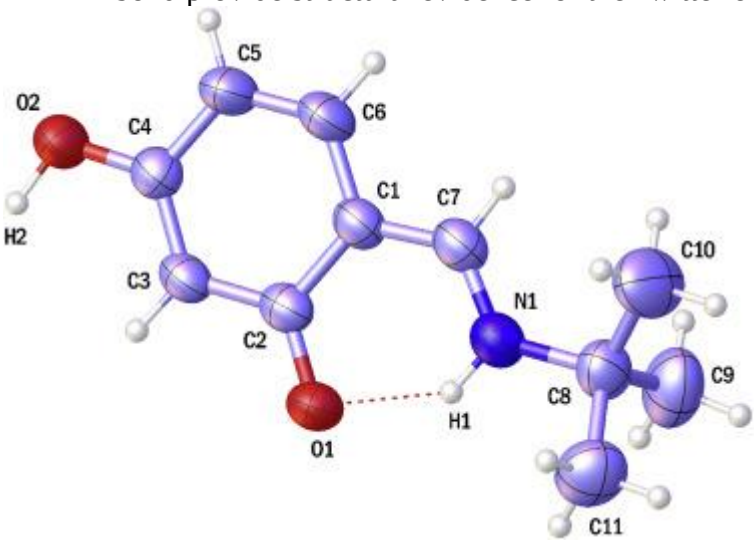

Fig. 3. ORTEP representation of **L²**. Displacement ellipsoids are drawn at the 30% probability level and H atoms are shown as small spheres of arbitrary radii. Intramolecular H-bond is illustrated by dashed line.

Scheme 2. Possible tautomeric forms for **L**[1] and **L**[2].

Intramolecular N H···O hydrogen bond between the NH^+ and the phenolate O^- generates an S(6) ring motif (Fig. 3; Table 3) which help to stabilize the planarity of the molecule [58]. The bond distances are in normal ranges and comparable with those found in related

structures [59], [60]. In the crystal packing, molecules are connected by O H···O hydrogen bonds, generating C(6) chains (Fig. 4) [58]. According to the hydrogen bonding classification [61], [62], these intramolecular and intermolecular hydrogen-bonding are moderate (mostly electrostatic) and strong (strongly covalent) interactions, respectively.

Table 3. Hydrogen-bond geometry (Å, °) for **L²**.

D—H···A	**D—H**	**H···A**	**D···A**	**D—H···A**	Empty Cell	**Symmetry code**
N(1) H(1)···O(1)	0.904(15)	1.875(15)	2.6233(17)	138.7	Intra	
O(2) H(2)···O(1)	0.965(19)	1.593(18)	2.5429(15)	167.1	Inter	−1/2 + x,1/2−y,−z

Note: D donor, A acceptor.

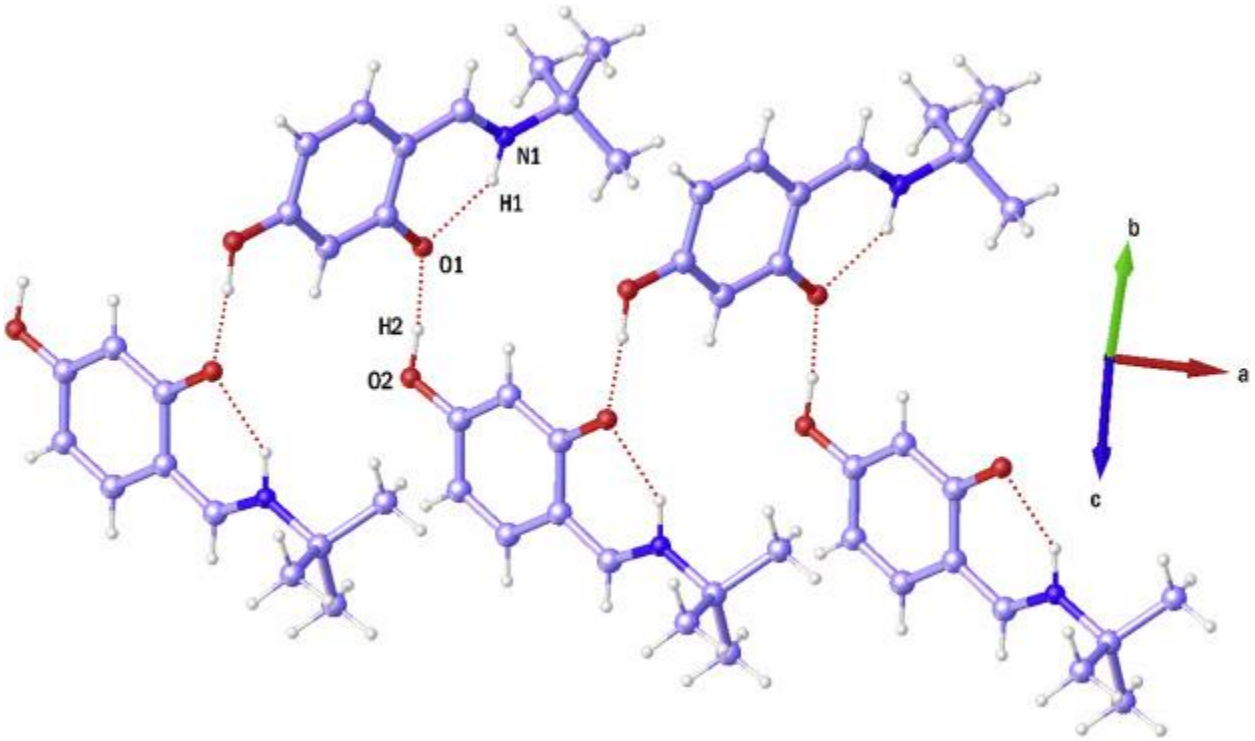

Fig. 4. Intramolecular and intermolecular hydrogen bond geometries for **L²** (Å,°).

3.2. UV–vis spectroscopy

UV–vis absorption spectroscopy is an effective and simple technique to study of the HSA-drug binding and to investigate the structural changes of protein upon its drug binding. The UV absorption spectra of HSA shows a strong absorption peak at about 220 nm resulted of the n→π* transition for the peptide bond of α-helix and a weak peak at 278 nm assigned to π→π* transition of the phenyl rings in aromatic acid residues (Trp, Tyr and Phe) [63]. Through addition of various amount of the Schiff base ligands (10×10^{-5} M), a hypochromic effect in spectrum of HSA is

observed (Fig. 5). This observation indicates that the aromatic amino acid residues of HSA in a hydrophobic cavity were exposed to an aqueous upon binding to the compounds. Moreover, observation of hypochromic effect in UV–vis spectra of HSA with increase amount of the synthesized ligands reveals the π–π stacking interaction between the aromatic rings of the compounds and the phenyl rings of aromatic acid residues [63].

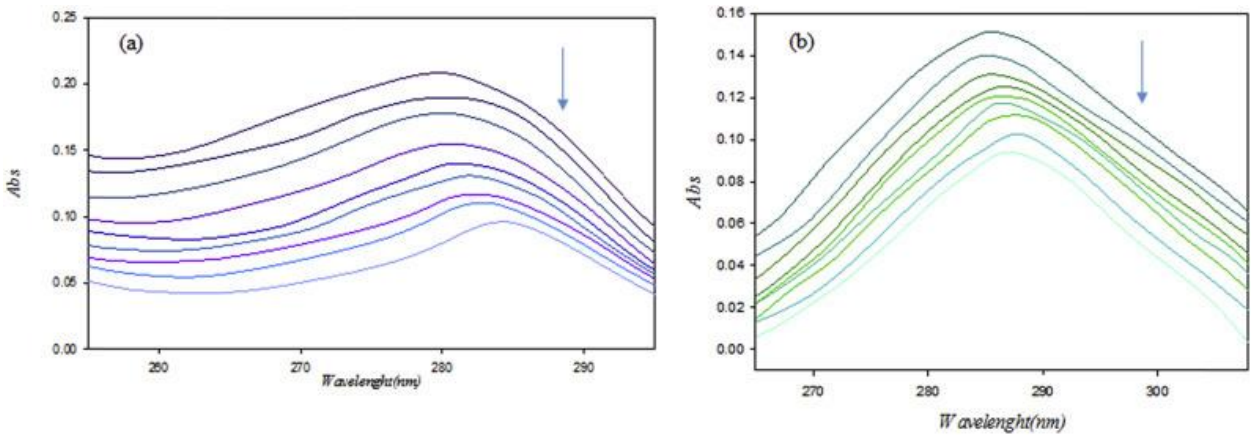

Fig. 5. Electronic absorption spectra of HSA (10 μM) in the absence and presence of various concentrations of (a) **L¹** and (b) **L²**.

To assess the binding ability of the Schiff base ligands with HSA, the intrinsic binding constant (K_b) was determined using Benesi–Hildebrand plot and the following equation [64], [65]:

$$\frac{1}{A-A_0} = \frac{1}{A_{max}-A} + \frac{1}{[M]} \times \frac{1}{K_b(A_{max}-A)} \quad (1)$$

where A_0 and A are the absorbance of HSA in the absence and presence of drug, respectively. A_{max} is the obtained absorbance at saturation and [M] is the concentration of drug. The plot of $1/(A\text{-}A_0)$ versus 1/[M] gives K_b as ratio of y-intercept to slop. The binding constants for **L¹** and **L²** are equal to 1.31×10^4 and 3.16×10^4, respectively (Fig. S3).

3.3. Fluorescence spectroscopy

Fluorescence quenching experiment has been performed to investigate the mechanism of interaction between HSA and the ligands. Although fluorescence of HSA protein is due to the presence of three amino acids, i.e. tryptophan (Trp), tyrosine (Tyr), and phenylalanine (Phe) residues, the intrinsic fluorescence of HSA comes from tryptophan [66].
The fluorescence intensity of protein was quenched through the addition of the synthesized ligands, revealing the interaction of the ligands and HSA takes place and leads to the changes of microenvironment around the Trp-214 residue in HSA [67], [68]. Fig. 6 represents the fluorescence quenching of 5 μM HSA at the presence of various amounts of the ligands (5×10^{-5} M). In order to determine the binding ability between the ligands and HSA, the Stern–Volmer quenching plot was obtained by monitoring the fluorescence quenching of HSA with increasing the concentration of the compounds according to the Stern–Volmer equation [67]:

$$F_0/F = 1 + K_{SV}[Q] = 1 + k_q\tau[Q] \quad (2)$$

where, F_0 and F are the fluorescence intensity of HSA in absence and presence of the compounds. K_{sv} is the Stern–Volmer quenching constant, k_q is the quenching rate constant of HSA and τ is the average lifetime of HSA without quencher which is typically equal to 10^{-8} s for biomacromolecules [38]. K_{sv} is determined from the plot of F_0/F vs. [Q] (Fig. 6). In the present study, the values of K_{sv} were obtained and presented in Table 4. Fluorescence quenching is classified to two mechanisms: static quenching and dynamic quenching. In the static mechanism, the fluorophore and the quencher collide together in the ground state while fluorophore and quencher collide together in the excited state in dynamic mechanism. Linearity of the Stern–Volmer plot indicates that quenching fluorescence has only one mechanism, dynamic or static [38]. In this study, the value of k_q was obtained and represented in Table 4 that is greater than limiting diffusion rate constant of the diffusional quenching for biopolymers (2×10^{10} $M^{-1}S^{-1}$). This observation supports that quenching fluorescence of HSA occurs by static mechanism [38]. In addition the changes in the absorption spectrum of HSA show the formation HSA-drug complex in the ground state, which is because of the change in the HSA structure. While dynamic quenching affects on the exited state and do not have impact on the absorption spectrum. Moreover, binding constant (K_b) of the ligands and HSA can be calculated by this experiment using following equation [38]:

$$\ln\left(\frac{F_0-F}{F}\right) = \ln K_b - n \ln[Q] \quad (3)$$

where, F_0 and F are the fluorescence intensity of HSA in absence and presence of Schiff base ligand, respectively. [Q] is the concentration of quencher that quencher is the synthesized ligand

here. "K_b" is obtained from the plot of ln ((F_0 F/F) versus Ln[Q]as a y-intercept. Furthermore, "n" which is the number of binding site per protein is slope of the plot. The value of n is nearly 1, indicating that the synthesized compounds bind to HSA with molar ratio of 1:1. The calculated results are shown in Table 4. The K_b value reveals that the **L²**-HSA complex is more stable than other one; in the other words, this is more available for drug–cell interaction. Moreover, this result is in good agreement with the UV–vis spectroscopy result.

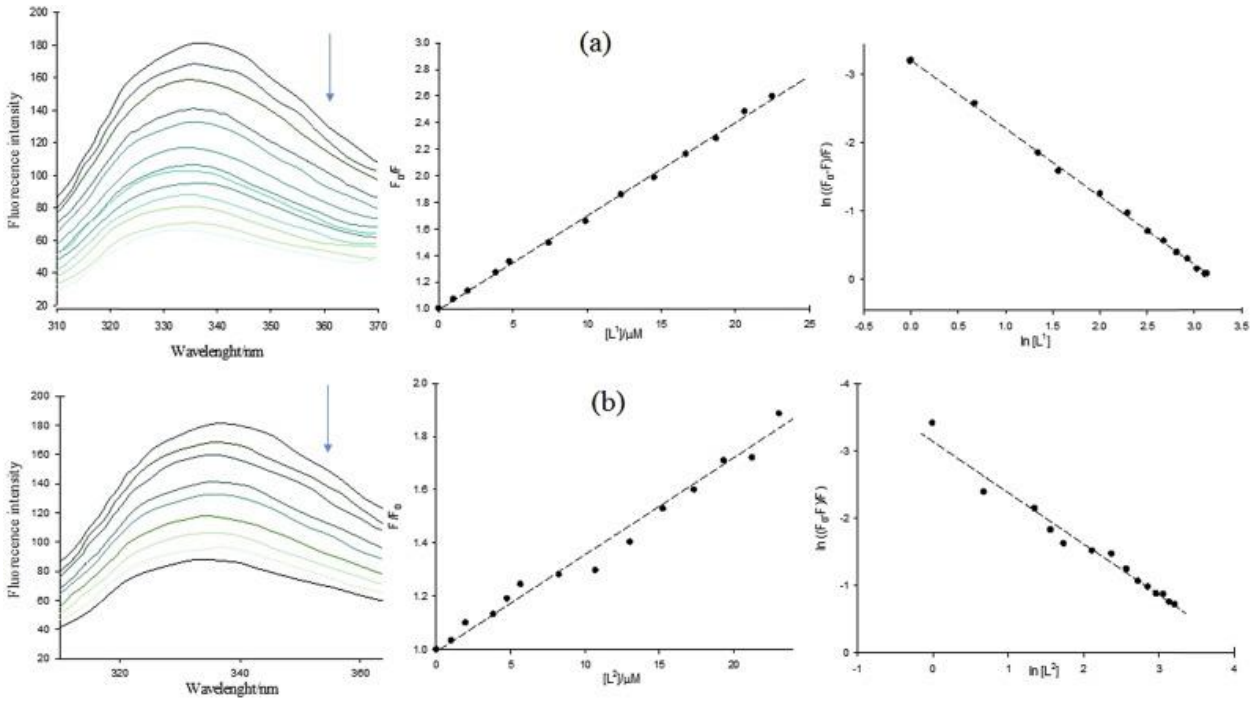

Fig. 6. Fluorescence quenching of HSA (5 μM) in the absence and presence of various concentrations of (a) **L[1]** and (b) **L[2]**.

Table 4. The HSA binding constant (K_b), the number of binding sites (n), the Stern–Volmer constant (K_{sv}) of the compounds, the quenching rate constant of HSA (k_q) and the obtained results from FRET theory for the compounds.

Ligand	K_{SV}	k_q	K_b	n	R_0 **(nm)**	r **(nm)**
L[1]	7.04×10^4	7.04×10^{12}	4.05×10^4	1	3.07	3.35
L[2]	3.63×10^4	3.63×10^{12}	4.33×10^4	0.76	1.30	1.57

In general, binding constant of a drug with a carrier protein such as HSA should be high enough to bind and transfer thought body. Moreover, in order to release a drug since arrival at its target, it should not be too high. With respect to above, HSA binding constants of these ligands are in a good range ($2–10 \times 10^4$) [69].

3.4. Energy transfer from HSA to ligands

Energy transfer between the ligands and HSA can provide valuable information about HSA-ligand binding. The fluorescence quenching of HSA upon the binding of ligands can be indicative of energy transfer between HSA and these compounds. This energy transfer can be explained by fluorescence resonance energy transfer (FRET) theory. FRET that also known as Förster's resonance energy transfer is an interaction between the excited molecule and its adjacent molecule. Upon this interaction, energy absorbed by donor molecule is transferred to an acceptor [70]. According to this theory, three conditions are required to energy transfer: (1) the donor should

have fluorescence, (2) the fluorescence emission spectrum of the donor and the UV–vis spectrum of the acceptor should have sufficient overlap (3) the small distance between donor and acceptor (<8 nm) [70]. The distance and efficiency of energy transfer (*E*) between tryptophan residue of protein (HSA) and ligand has been calculated using this theory through the following equation:

$$\mathrm{E} = 1 - \frac{F}{F_0} = \frac{R_0^6}{R_0^6 + r^6} \tag{4}$$

where F_0 and F are fluorescence intensities of HSA in the absence and presence of ligands, respectively and R_0 is the critical distance when the transfer efficiency is 50%; r is the distance between donor and acceptor. R_0 can be calculated by Eq. (5) [71].

$$R_0^6 = 8.79 \times 10^{-25} K^2 N^{-4} J\varphi \tag{5}$$

In the above equation, the term K^2 is the orientation factor of the dipoles; N is the refracted index of medium, J is the overlap integral of the fluorescence spectrum of the donor with absorption spectrum of the acceptor and φ is the fluorescence quantum yield of the donor. The value of J can be calculated by the following expression:

$$J = \frac{F(\lambda)\varepsilon(\lambda)\lambda^4\Delta\lambda}{\sum F(\lambda)\Delta(\lambda)} \tag{6}$$

where, $F(\lambda)$ is the fluorescence intensity of the donor in the absence of the acceptor at wavelength λ and ε is the molar absorption coefficient of the acceptor at λ. In the present case, $K^2 = 2/3$, $N = 1.336$ and $\varphi = 0.15$ for HSA. Therefore, according to Eqs. (4), (5), (6) the parameters for the synthesized ligands were calculated (Table 4). Fig. 7 represents the overlap of the fluorescence emission spectrum of HSA (5 μM) and the UV–vis spectrum of ligands (5 μM). The values of r for all the ligands are less than 8 nm and "$0.5\ R_0 < r < 1.5\ R_0$", suggesting energy transfer from HSA to the Schiff base ligands occurs with high probability. Furthermore, the higher values of r than R_0, indicating the presence of a static quenching mechanism in the interaction of HSA and compounds [72].

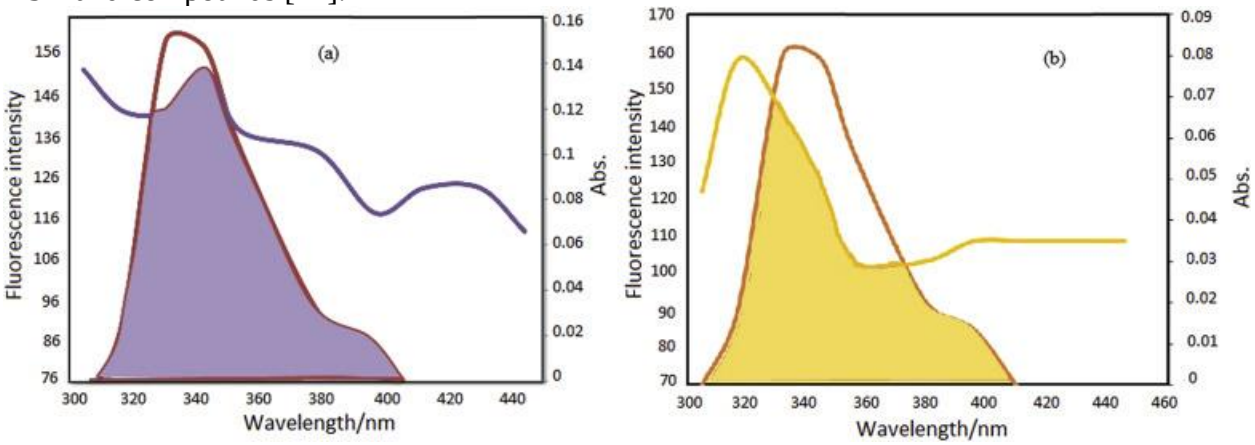

Fig. 7. Spectral overlap of the HSA fluorescence with the (a) $\mathbf{L^1}$ and (b) $\mathbf{L^2}$ absorption spectrum. [HSA] = [L] = 5 μM, λ_{ex} = 295 nm.

3.5. Molecular docking studies

It has been confirmed that the major factor affecting on the distribution, metabolism, the free concentration and the elimination rate of drugs is the binding affinity of drugs to HSA. Moreover, the half-life of drugs depends on their HSA-binding that effects on the dosage of drugs [73]. Therefore, the study of interaction between HSA and drugs is essential to investigate the pharmacokinetics and availability of drugs in tissues. HSA as the most abundant carrier protein comprises three α-helical domains (I, II and III), each containing two subdomains (A and B) [74]. The previous crystal structure studies showed that many drugs bind to one of the three binding sites located in subdomains IIA, IIIA and IB. In this work, the synthesized ligands were docked to the crystal structure of HSA. The obtained results from molecular docking showed that two ligands bind to the IB subdomain of HSA. Also, the affinity of $\mathbf{L^2}$ is higher than the $\mathbf{L^1}$. The standard Gibbs free energies for binding of ligands to HSA are −5.63 and −5.82 kcal mol^{-1} for $\mathbf{L^1}$ and $\mathbf{L^2}$, respectively. The results indicated that TYR161 and ARG117 amino acid residues are involved in the hydrogen bond interaction in the HSA-$\mathbf{L^1}$ system. Also, ASP108 and TYR148 amino acid residues are involved in the hydrogen bond interaction in the HSA-$\mathbf{L^2}$ complex. The results of docking are presented in Fig. 8, Fig. 9. The docking results are in good agreement with the experimental results and reveal important interactions between Schiff base ligands and HSA. Thus it can be concluded that the interaction of $\mathbf{L^1}$ and $\mathbf{L^2}$ with HSA is not mainly hydrophobic and the phenolic OH groups in the structure of ligands have a significant role in the binding process.

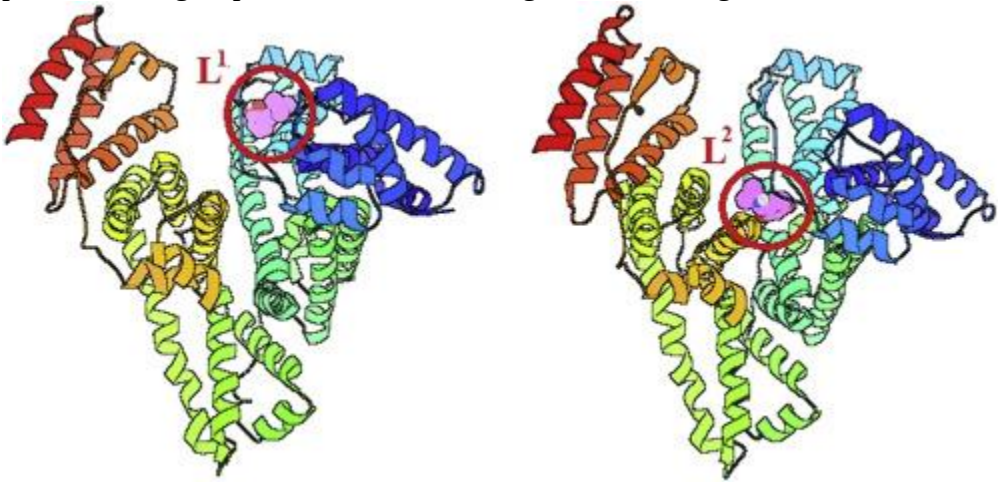

Fig. 8. L^1 and $\mathbf{L^2}$ docked in HSA using AutoDock. Ligands, depicted as a surface model, and HSA, represented in cartoon ribbon (The red circles show the ligands).

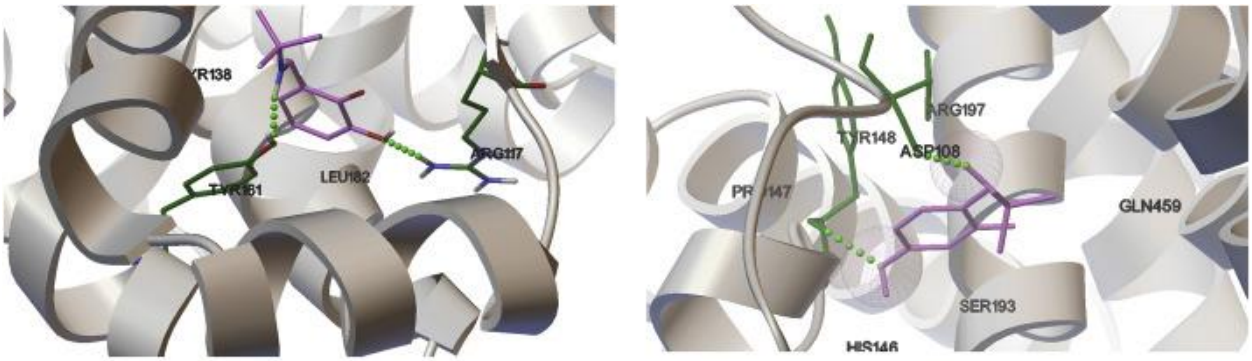

(a) (b)

Fig. 9. The docking poses of the HSA–ligand complexes. a) **L**[1] and b) **L**[2]. Hydrogen bond interactions showed as spheres.

3.6. Analysis of the dynamics trajectories

The beginning structures for the MD analyses were selected from the conformations with lowest docking energies. The trajectories were analyzed in terms of root mean square deviation (RMSD), radius of gyration (R_g), and root mean square fluctuation (RMSF) using the GROMACS routines.

3.7. Root mean square deviation

The stability of trajectories for HSA–ligands was examined using the RMSD of the backbone of HSA (Fig. 10). A glance at the analysis in Fig. 10 shows that the RMSD of all systems reached equilibrium and fluctuated around 0.44 and 0.39 nm for **L**[1] and **L**[2], respectively at about 7500 ps. This means that HSA-**L** complexes are well equilibrated and RMSD has low fluctuation around its mean value.

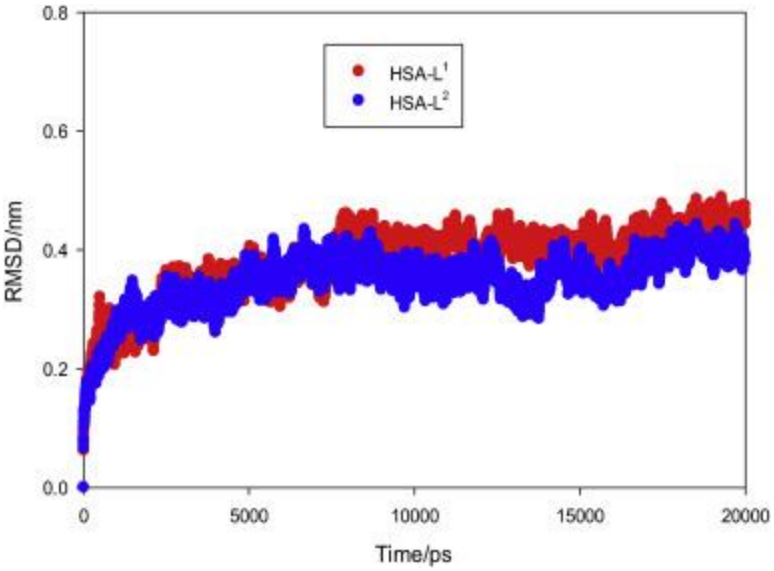

Fig. 10. Time dependence of RMSD. RMSD values for HSA–ligand complexes.

3.8. Radius of gyration

The R_gs for all systems were also determined and plotted against simulation time to study the protein compactness (Fig. 11) showed that all of the systems stabilized after about 8000 ps, indicating that the MD simulation equilibrated after 8000 ps. It can be clearly seen that the R_g was larger upon binding of the **L²** than for **L¹** suggesting a less compact structure after the binding of **L²** Schiff base ligand to HSA. Also, Fig. 11 shows that the R_g value of HSA decreases upon the complexation with **L¹** and **L²**. This indicates that the environment of HSA changes during its interaction with Schiff base ligands.

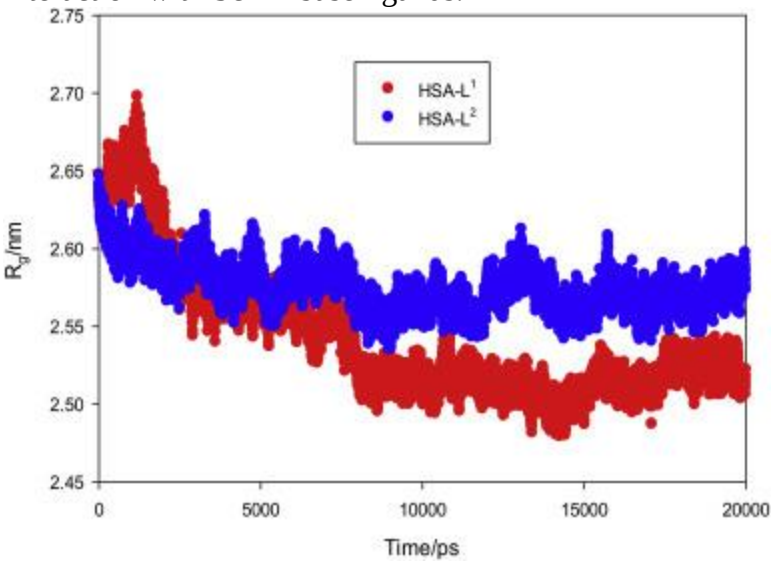

Fig. 11. Time evolution of the radius of gyration (R_g) during 20,000 ps of MD simulation of HSA–ligand complexes.

3.9. Root mean square fluctuation

The mobility of the HSA residues was evaluated by analysis of the RMSF of the Cα atoms of HSA in the presence of the Schiff base ligands (Fig. 12). The results indicate that the residues that were in contact with the ligands are the most stable and have low RMSF values.

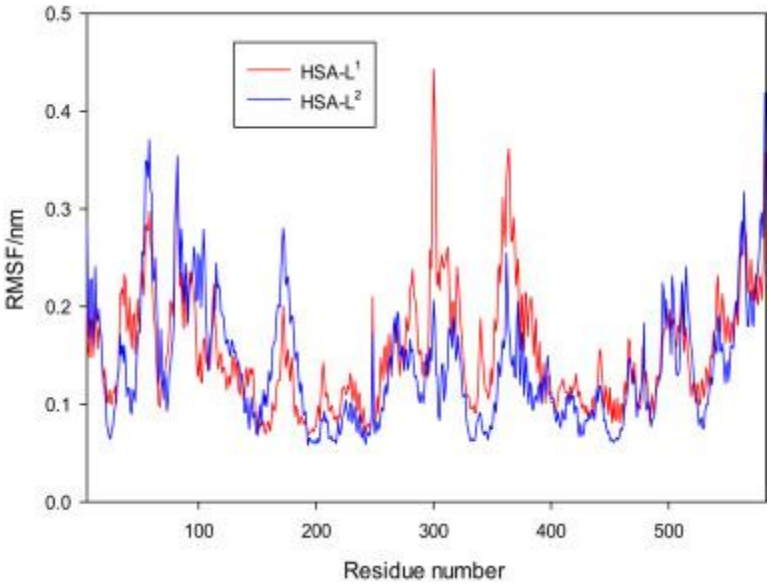

Fig. 12. The RMSF values of HSA–ligand complexes were plotted against residue numbers.

In addition, the RMSF of the atomic positions of the Schiff base ligands was calculated to examine their conformational variations (Fig. 13). The results indicate that the ligands atoms showed limited fluctuations (<0.14 nm). Hence, it can be concluded that the interactions of HSA and the Schiff base ligands were stable during the simulation time.

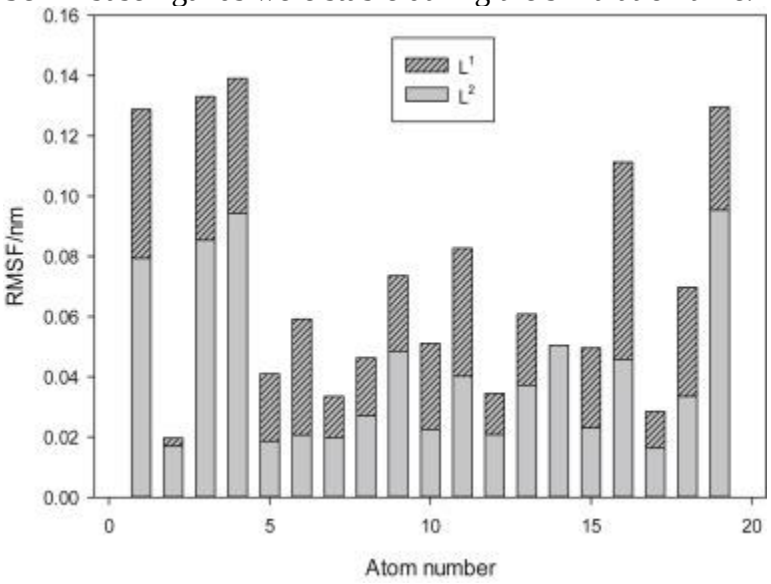

Fig. 13. RMSF values of Schiff base ligands were plotted against atom numbers.

4. Conclusions

In this study, two new *o*-hydroxy Schiff-bases compounds, **L^1** and **L^2**, have been synthesized from reaction of 2,3-dihydroxybenzaldehyde and 2,4-dihydroxybenzaldehyde with *tert*-butylamine. The synthesized compounds have been investigated by elemental analysis and FT-IR, ^{1}H and ^{13}C

NMR spectroscopy. The structure of **L²** has been also confirmed by X-ray crystallography. The crystal structure of **L²** showed that the compound exists as a zwitterionic form in the solid state, with the H atom of the phenol group being transferred to the imine N atom. The HSA binding of the synthesized compounds were evaluated using experimental methods including fluorescence quenching and UV–vis spectroscopy. The computational methods (molecular docking and molecular dynamics simulation methods) were also carried out to investigate more details. The obtained results from both experimental and theoretical methods indicate that the compounds bind to HSA as **L²** > **L¹**. The obtained results from UV–vis spectroscopy and fluorescence quenching represent that all the synthesized compounds bind to HSA with binding constants about 4×10^4 M^{-1} that is appropriate value for drugs. The results of fluorescence experiment as well as the changes in the absorption spectrum of HSA upon addition of the compounds show that the HSA-compound complexes formed in the ground state. The synthesized ligands bind to HSA with molar ratio of 1:1. Moreover the binding distance between the donor (HSA) and the acceptors (the ligands) was evaluated based on the FRET theory and the results indicated that the quenching of HSA by the synthesized compounds was static quenching processes.

In addition, the binding propensity of the compounds to HSA was investigated by computational methods (Molecular docking and molecular dynamics simulation methods). Molecular docking studies revealed that hydrogen bond and hydrophobic interactions have major role in the binding of these Schiff base ligands to HSA. The presence of the hydrogen bond gives additional stabilization to the HSA-ligands systems. Also, the details of HSA binding properties of the compounds on the molecular level were obtained by this method.

To investigate HSA-binding of the compounds more accurately, the molecular dynamics simulation method was carried out. MD simulation studies showed the stabilization of HSA–ligand complexes at around 8 ns It can be clearly seen that R_g decrease upon binding of Schiff base ligands, suggesting a more compact structure after the binding of these two ligands to HSA. In addition, the environment of HSA changes slightly during its interaction with **L¹** and **L²**. Furthermore, the profiles of atomic fluctuations showed that the interactions of HSA and Schiff base ligands were stable during the simulation time.

Acknowledgment

Support for this research by the University of Isfahan and Islamic Azad University (Qeshm branch) is acknowledged.

Appendix A. Supplementary data

The following is the supplementary data related to this article:

CCDC 1448114 contains the supplementary crystallographic data for **L²**. This data can be obtained free of charge via http://www.ccdc.cam.ac.uk/conts/retrieving.html, or from the Cambridge Crystallographic Data Centre, 12 Union Road, Cambridge CB2 1EZ, UK; fax: (+44) 1223-336-033; or e-mail: deposit@ccdc.cam.ac.uk.

References

[1] D.K. Dey, S.P. Dey, A. Elmali, Y. Elerman, J. Mol. Struct. 562 (2001) 177e184.

[2] T. H€okelek, Z. Kılıç, M. Isıklan, M. Toy, J. Mol. Struct. 523 (2000) 61e69.
[3] H. Karabıyık, N. Ocak-_Iskeleli, H. Petek, Ç. Albayrak, E. A_gar, J. Mol. Struct. 873 (2008) 130e136.
[4] A.M. Farag, T.S. Guan, H. Osman, M. Hemamalini, H.K. Fun, Acta Cryst. E 66 (2010) o2466.
[5] H. Petek, Ç. Albayrak, N.O. _Iskeleli, E. A_gar, _I. S¸ enel, J. Chem. Crystallogr.. 37(2007) 285e290.
[6] E. Hadjoudis, I.M. Mavridis, Chem. Soc. Rev. 33 (2004) 579e588.
[7] A. Filarowski, A. Koll, M. Rospenk, I. Krol-Starzomska, J. Phys. Chem. A 109 (2005) 4464e4473.
[8] P.M. Dominiak, E. Grech, G. Barr, S. Teat, P. Mallinson, K. Wozniak, Chem. Eur. J. 9 (2003) 963e970.
[9] A. Filarowski, I. Majerz, J. Phys. Chem. A 112 (2008) 3478e3485.
[10] A. Filarowski, A. Koll, T. Glowiak, J. Chem. Soc. Perkin Trans. 2 (2002) 835e842.
[11] Y. Zhang, Z.J. Guo, X.Z. You, J. Am. Chem. Soc. 123 (2001) 9378e9387.
[12] E. Hadjudis, et al., Photochromism, Elsevier, Amsterdam, 1990, p. p 685.
[13] Z. Kazemi, H. Amiri Rudbari, V. Mirkhani, M. Sahihi, M. Moghadam, S. Tangestaninejad, I. Mohammadpoor-Baltork, J. Mol. Struct. 1096 (2015) 110e120.
[14] S. Tabassum, M. Ahmad, M. Afzal, M. Zaki, P.K. Bharadwaj, J. Photochem. Photobiol. B Biol. 140 (2014) 321e331.
[15] M. Yıldız, €O. Karpuz, C.T. Zeyrek, B. Boyacıo_glu, H. Dal, N. Demir, N. Yıldırım, H. Ünver, J. Mol. Struct. 1094 (2015) 148e160.
[16] B. Barare, M. Yıldız, G. Alpaslan, N. Dilek, H. Ünver, S. Tadessea, K. Aslan, Sens. Actuat. B Chem. 215 (2015) 52e61.
[17] P. Li, M.J. Niu, M. Hong, S. Cheng, J.M. Dou, J. Inorg. Biochem. 137 (2014) 101e108.
[18] J. Lu, Q. Sun, J.L. Li, L. Jiang, W. Gu, X. Liu, J.L. Tian, S.P. Yan, J. Inorg. Biochem. 137 (2014) 46e56.
[19] S. Menati, H. Amiri Rudbari, M. Khorshidifard, F. Jalilian, J. Mol. Struct. 1103 (2016) 94e102.
[20] M. Khorshidifard, H. Amiri Rudbari, B. Askari, M. Sahihi, M. Riahi Farsani, F. Jalilian, G. Bruno, Polyhedron 95 (2015) 1e13.
[21] H. Amiri Rudbari, M. Khorshidifard, B. Askari, N. Habibi, G. Bruno, Polyhedron 100 (2015) 180e191.
[22] M. Khorshidifard, H. Amiri Rudbari, Z. Kazemi-Delikani, V. Mirkhani, R. Azadbakht, J. Mol. Struct. 1081 (2015) 494e505.
[23] H. Keypour, A. Shooshtari, M. Rezaeivala, M. Bayat, H. Amiri Rudbari, Inorg. Chim. Acta 440 (2016) 139e147.
[24] H. Keypour, A. Shooshtari, M. Rezaeivala, F. Ozturk Kup, H. Amiri Rudbari, Polyhedron 97 (2015) 75e82.
[25] G. Grivani, V. Tahmasebi, K. Eskandari, A. Dehno Khalaji, G. Bruno, H. Amiri Rudbari, J. Mol. Struct. 1054 (2013) 100e106.
[26] H. Iranmanesh, M. Behzad, G. Bruno, H. Amiri Rudbari, H. Nazari, A. Mohammadi, O. Taheri, Inorg. Chim. Acta 395 (2013) 81e88.
[27] M. Pooyan, A. Ghaffari, M. Behzad, H. Amiri Rudbari, G. Bruno, J. Coord. Chem.

66 (2013) 4255e4267.
[28] A. Ghaffari, M. Behzad, M. Pooyan, H. Amiri Rudbari, G. Bruno, J. Mol. Struct. 1063 (2014) 1e7.
[29] H. Keypour, M. Shayesteh, D. Nematollahi, L. Valencia, H. Amiri Rudbari, J. Coord. Chem. 63 (2010) 165.
[30] G. Grivani, M. Vakili, A.D. Khalaji, G. Bruno, H. Amiri Rudbari, M. Taghavi, V. Tahmasebi, J. Mol. Struct. 1072 (2014) 77e83.
[31] G. Grivani, G. Bruno, H. Amiri, A.D. Khalaji, P. Pourteimouri, Inorg. Chem. Commun. 18 (2012) 15e20.
[32] H. Keypour, R. Azadbakht, H. Amiri Rudbari, A. Heydarinekoo, H.R. Khavasi, Trans. Met. Chem. 34 (2009) 835e839.
[33] H. Amiri Rudbari, M. Riahi Farsani, S. Lanza, G. Bruno, B. Yadollahi, C. R. Chim. 18 (2015) 391e398.
[34] (a) COSMO, Version 1.60, Bruker AXS Inc., Wisconsin, Madison, 2005;
(b) SAINT, Version 7.06A, Bruker AXS Inc., Wisconsin, Madison, 2005;
(c) SADABS, Version 2.10, Bruker AXS Inc., Wisconsin, Madison, 2005.
[35] M.C. Burla, R. Caliandro, M. Camalli, B. Carrozzini, G.L. Cascarano, L. De Caro, C. Giacovazzo, G. Polidori, R. Spagna, J. Appl, Crystallogr 38 (2005) 381e388.
[36] G.M. Sheldrick, SHELXL-97, University of G€ottingen, G€ottingen, Germany, 1997.
[37] O.V. Dolomanov, L.J. Bourhis, R.J. Gildea, J.A.K. Howard, H. Puschmann, OLEX2: A complete structure solution, refinement and analysis program, J. Appl. Crystallogr. 42 (2009) 339e341.
[38] T. Hosseinzadeh Sanatkar, H. Hadadzadeh, Z. Jannesari, T. Khayamian, M. Ebrahimi, H. Amiri Rudbari, M. Torkzadeh-Mahani, M. Anjomshoa, Inorg. Chim. Acta 423 (2014) 256e272.
[39] M.J. Frisch, G.W. Trucks, H.B. Schlegel, G.E. Scuseria, M.A. Robb, J.R. Cheeseman, G. Scalmani, V. Barone, B. Mennucci, G.A. Petersson, H. Nakatsuji, M. Caricato, X. Li, H.P. Hratchian, A.F. Izmaylov, J. Bloino, G. Zheng, J.L. Sonnenberg, M. Hada, M. Ehara, K. Toyota, R. Fukuda, J. Hasegawa, M. Ishida, T. Nakajima, Y. Honda, O. Kitao, H. Nakai, T. Vreven, J.A. Montgomery Jr., J.E. Peralta, F. Ogliaro, M. Bearpark, J.J. Heyd, E. Brothers, K.N. Kudin, V.N. Staroverov, R. Kobayashi, J. Normand, K. Raghavachari, A. Rendell, J.C. Burant, S.S. Iyengar, J. Tomasi, M. Cossi, N. Rega, J.M. Millam, M. Klene, J.E. Knox, J.B. Cross, V. Bakken, C. Adamo, J. Jaramillo, R. Gomperts, R.E. Stratmann, O. Yazyev, A.J. Austin, R. Cammi, C. Pomelli, J.W. Ochterski, R.L. Martin, K. Morokuma, V.G. Zakrzewski, G.A. Voth, P. Salvador, J.J. Dannenberg, S. Dapprich, A.D. Daniels, O. Farkas, J.B. Foresman, J.V. Ortiz, J. Cioslowski, D.J. Fox, Gaussian Development Version, Revision B.01, Gaussian. Inc., Wallingford CT, 2009.
[40] A.D.J. Becke, Chem. Phys. 98 (1993) 5648e5652.
[41] M.M. Francl, W.J. Pietro, W.J. Hehre, J.S. Binkley, M.S. Gordon, D.J. DeFrees, J.A. Pople, J. Chem. Phys. 77 (1982) 3654e3665.
[42] G.M. Morris, D.S. Goodsell, R.S. Halliday, R. Huey, W.E. Hart, R.K. Belew, A.J. Olson, J. Comput. Chem. 19 (1998) 1639e1662.
[43] H.J.C. Berendsen, D. Van der Spoel, R. Van Drunen, Comput. Phys. Commun. 91

(1995) 43e56.
[44] E. Lindah, B. Hess, D. Van der Spoel, J. Mol. Model 7 (2001) 306e317.
[45] W.F. Van Gunsteren, S.R. Billeter, A.A. Eising, P.H. Hünenberger, P.K.H.C. Krüger, A.E. Mark, W.R.P. Scott, I.G. Tironi, Biomolecular Simulation: the GROMOS96 Manual and User Guide, Vdf Hochschulverlag AG, Zürich1996.
[46] W.F. Van Gunsteren, X. Daura, A.E. Mark, Encyclopedia of Computational Chemistry, Wiley and Sons, P. Von Rague Schleyer, Chichester, UK, 1998.
[47] A.W. Schuttelkopf, D.M.F. Van Aalten, Acta Crystallogr. 60 (2004) 1355e1363.
[48] H.J.C. Berendsen, J.P.M. Postma, W.F. Van Gunstetren, J. Hermans, in: B. Pullman (Ed.), Intermolecular Forces, Reidel, Dordrecht, The Netherlands, 1981.
[49] H.J.C. Berendsen, J.P.M. Postma, W.F. Van Gunsteren, A. DiNola, J.R. Haak, J. Chem. Phys. 81 (1984) 3684e3690.
[50] T. Darden, D. York, L. Pedersen, J. Chem. Phys. 98 (1993) 10089e10092.
[51] U. Essmann, L. Perera, M.L. Berkowitz, T. Darden, H. Lee, L.G. Pedersen, J. Chem. Phys. 103 (1995) 8577e8593.
[52] M. Yıldız, Z. Kılıç, T. H€okelek, J. Mol. Struct. 441 (1998) 1e10.
[53] H. Nazır, M. Yıldız, H. Yılmaz, M.N. Tahir, D. Ülkü, J. Mol. Struct. 524 (2000) 241e250.
[54] G. Alpaslan, M. Macit, A. Erd€onmez, O. Büyükgüng€or, J. Mol. Struct. 997 (2011) 70e77.
[55] B. Kosar, Ç. Albayrak, M. Odabasoglu, O. Büyükgüng€or, J. Mol. Struct. 989 (2011) 31e37.
[56] B. Kosar, C. Albayrak, Spectrochim. Acta Part A 78 (2011) 160e167.
[57] A. €Ozek, Ç. Albayrak, M. Odabaso_glu, O. Büyükgüng€or, Acta Crystallogr. C 63 (2007) o177eo180.
[58] J. Bernstein, R.E. Davis, L. Shimoni, N.L. Chang, Angew. Chem. Int. Ed. 34 (1995) 1555e1573.
[59] N.E. Eltayeb, S.G. Teoh, S. Chantrapromma, H.K. Fun, Acta Cryst. E66 (2010) o934eo935.
[60] A.K. Baghdouche, S. Mosbah, Y. Belhocine, L. Bencharif, Acta Cryst. E70 (2014) o676.
[61] T. Steiner, Angew. Chem. Int. Ed. 41 (2002) 48e76.
[62] G.R. Desiraju, T. Steiner, The Weak Hydrogen Bond in Structural Chemistry and Biology, Oxford University Press Inc., New York, 1999.
[63] X.B. Fu, D.D. Liu, Y. Lin, W. Hu, Z.W. Mao, X.Y. Le, Dalton Trans. 43 (2014) 8721e8737.
[64] A. Das, G.S. Kumar, RSC Adv. 4 (2014) 33082e33090.
[65] N.U.H. Khan, N. Pandya, N.C. Maity, M. Kumar, R.M. Patel, R.I. Kureshy, S.H.R. Abdi, S. Mishra, S. Das, H.C. Bajaj, Eur. J. Med. Chem. 46 (2011) 5074e5085.
[66] M. Ganeshpandian, R. Loganathan, E. Suresh, A. Riyasdeen, M.A. Akbarsha, M. Palaniandavar, Dalton Trans. 43 (2014) 1203e1219.
[67] E.M. Mrkali_c, R.M. Jeli_c, O.R. Klisuri_c, Z.D. Matovi_c, Dalton Trans. 43 (2014) 15126e15137.
[68] Y. Wang, H. Zhang, G. Zhang, W. Tao, S. Tang, J. Lumin 126 (2007) 211e218.

[69] M. Kyropoulou, C.P. Raptopoulou, V. Psycharis, G. Psomas, Polyhedron 61 (2013) 126e136.
[70] N. Fani, A.K. Bordbar, Y. Ghayeb, Spectrochim. Acta Part A 103 (2013) 11e17.
[71] S. Huang, F. Zhu, Q. Xiao, Q. Zhou, W. Su, H. Qiu, B. Hu, J. Shenga, C. Huang, RSC Adv. 4 (2014) 36286e36300.
[72] F.Y. Wu, F.Y. Xie, Y.M. Wu, J.I. Hong, Spectrochim. Acta Part A 70 (2008) 1127e1133.
[73] S. Ranjbar, Y. Shokoohinia, S. Ghobadi, N. Bijari, S. Gholamzadeh, N. Moradi, M.R. Ashrafi-Kooshk, A. Aghaei, R. Khodarahmi, Sci. World J. 2013 (2013) 1e13.
[74] F. Zsila, Mol. Pharm. 10 (2013) 1668e1682.